Magnetoelastic phenomena in antiferromagnetic uranium intermetallics: The UAu_2Si_2 case

M. Vališka,[1,2,*] H. Saito,[3] T. Yanagisawa,[3] C. Tabata,[4] H. Amitsuka,[3] K. Uhlířová,[1] J. Prokleška,[1] P. Proschek,[1] J. Valenta,[1] M. Míšek,[5] D. I. Gorbunov,[6] J. Wosnitza,[6,7] and V. Sechovský[1]

[1]*Faculty of Mathematics and Physics, Charles University, DCMP, Ke Karlovu 5, CZ-12116 Praha 2, Czech Republic*
[2]*Institut Laue Langevin, 71 Avenue des Martyrs, CS 20156, F-38042 Grenoble Cedex 9, France*
[3]*Graduate School of Science, Hokkaido University, Sapporo 060-0810, Japan*
[4]*Institute of Materials Structure Science, High Energy Accelerator Organization, Tsukuba 305-0801, Japan*
[5]*Institute of Physics, ASCR v.v.i, Na Slovance 2, 182 21, Prague, Czech Republic*
[6]*Hochfeld-Magnetlabor Dresden (HLD-EMFL), Helmholtz-Zentrum Dresden-Rossendorf, 01328 Dresden, Germany*
[7]*Institut für Festkörper- und Materialphysik, TU Dresden, 01062 Dresden, Germany*

(Received 1 May 2018; revised manuscript received 1 November 2018; published 28 November 2018)

Thermal expansion, magnetostriction, and magnetization measurements under magnetic field and hydrostatic pressure were performed on a UAu_2Si_2 single crystal. They revealed a large anisotropy of magnetoelastic properties manifested by prominent length changes, leading to a collapse of the unit-cell volume accompanied by breaking the fourfold symmetry (similar to that in URu_2Si_2 in the hidden-order state) in the antiferromagnetic state as consequences of strong magnetoelastic coupling. The magnetostriction curves measured at higher temperatures confirm a bulk character of the 50 K weak ferromagnetic phase. The large positive pressure change of the ordering temperature predicted from Ehrenfest relation contradicts the more than an order of magnitude smaller pressure dependence observed by the magnetization and specific heat measured under hydrostatic pressure. A comprehensive magnetic phase diagram of UAu_2Si_2 in magnetic field applied along the c axis is presented. The ground-state antiferromagnetic phase is suppressed by a field-induced metamagnetic transition that changes its character from second to first order at the tricritical point.

DOI: 10.1103/PhysRevB.98.174439

I. INTRODUCTION

The anharmonic lattice vibrations due to the asymmetric bonding potential lead to increasing equilibrium interatomic distances with rising temperature in solids. The corresponding thermal expansion is a monotonously increasing function of temperature. The anisotropy of bonding within a crystal lattice causes an anisotropy of thermal expansion, which is manifested by different temperature dependences of the linear thermal expansion $(\Delta l/l)_i$ along the different crystallographic axes, i. The thermal expansion of metals includes also a conduction-electron contribution. This plays a considerable role at low temperatures where the phonon term almost vanishes.

The magnetostructural coupling, reflecting the interplay between the spin and lattice degrees of freedom, brings additional contributions to the thermal expansion in magnetic compounds. The magnetocrystalline anisotropy leads to anisotropic magnetic contributions to the thermal expansion. Magnetic materials then exhibit unusual thermal-expansion behavior, especially in a magnetically ordered state.

The thermal expansion, similar to the specific heat, is thus a useful probe for investigations of thermodynamic phenomena in magnetic materials (without applying magnetic field). The specific heat has only bulk character, whereas the thermal expansion enables us to study also the anisotropy of thermodynamic properties.

The spatially extended uranium $5f$-electron wave functions in solids considerably interact with the overlapping $5f$ orbitals of the nearest-neighbor U ions and the $5f$-electron states hybridize with valence-electron states of nonuranium ligands ($5f$-ligand hybridization [1]) and the $5f$ electrons even participate in bonding [2,3]. The exchange interactions that are coupling the uranium $5f$-electron magnetic moments in U antiferromagnets are strongly anisotropic. The direct exchange interactions are due to the $5f$-$5f$ orbitals' overlap. The anisotropy of these, typically ferromagnetic (FM), interactions and as well as the magnetocrystalline anisotropy are determined by the arrangement of the nearest-neighbor U ions in the lattice. The antiferromagnetic (AFM) interactions in U compounds are usually mediated by the anisotropic $5f$-ligand hybridization. The magnetoelastic coupling then produces highly anisotropic magnetic contributions to the thermal expansion and magnetostriction, especially in U antiferromagnets.

The anisotropy of magnetoelastic phenomena is a subject of numerous papers on U magnetics. Most frequently, they have been dedicated to the intriguing properties of URu_2Si_2, the most thoroughly studied uranium compound during more than the last three decades. There were no doubts about bulk superconductivity in URu_2Si_2 below 1.5 K since the earliest stage of research of this compound. Interpretation of the huge specific-heat peak and the Cr-like anomaly of electrical resistivity both at 17.5 K were, however, always a

*michal.valiska@gmail.com

subject of dispute. First, these were interpreted in terms of a transition to a weak itinerant antiferromagnetism [4], static charge-density wave (CDW), or spin-density wave (SDW) transition [5] or a local U-moment antiferromagnetism [6]. Neither long-range magnetic order nor any sign of a static CDW or SDW formation below 17.5 K has been confirmed by microscopic methods, however. Within time, the term "hidden order" (HO) was introduced to describe the unknown ordered state which allows unconventional superconductivity to occur at 1.5 K. URu_2Si_2 exhibits a nonmagnetic, nonstructural HO phase transition at $T_{HO} = 17.5$ K where the order parameter and elementary excitations so far could not be determined by microscopic experiments and only dynamical magnetic fluctuations are observed. Comprehensive information on the physics of URu_2Si_2 can be found in Ref. [7] and references therein. The volume of this compound reduces considerably below T_{HO} as manifested by a sharp positive peak in the thermal-expansion coefficient at T_{HO}. The volume reduction of the tetragonal structure is due to the basal-plane shrinkage. The simultaneous lattice expansion along the c axis is too small to compensate the negative basal-plane effect [8–11]. The possibility of a slight orthorhombic distortion of the tetragonal lattice at temperatures below T_{HO} plays an important role in the physics of URu_2Si_2. We will come back to this point in the Discussion section.

The influence of anisotropic exchange interactions on the anisotropy of the thermal expansion in U antiferromagnets is manifested by the magnetoelastic behavior of two other UT_2X_2 (T: transition metal; X: p-electron metal) compounds with the tetragonal $ThCr_2Si_2$ structure, UCo_2Si_2 [12,13], and UNi_2Si_2 [14], and several antiferromagnets from the family of hexagonal UTX compounds crystalizing in the ZrNiAl structure. In both structures, the nearest U-U neighbors are located in the basal plane where the U magnetic moments are coupled ferromagnetically. All these compounds exhibit a strong uniaxial anisotropy fixing the U moments to the c axis, which is the easy magnetization direction. The AFM structures in these materials are built of the FM basal-plane layers antiferromagnetically coupled along the c axis. The thermal expansion below the Néel temperature (T_N) in these antiferromagnets (similar to URu_2Si_2 below T_{HO}) is strongly anisotropic as well as the magnetostriction accompanying field-induced metamagnetic transitions from the AFM to paramagnetic state. The corresponding a- and c-axis linear thermal expansions $(\Delta l/l)_a$ and $(\Delta l/l)_c$, respectively, have in all cases opposite signs. The volume thermal expansion calculated according to

$$\Delta V/V = 2 \cdot (\Delta l/l)_a + (\Delta l/l)_c \qquad (1)$$

for the UT_2X_2 compounds is small as a result of compensation of the opposite-sign linear expansions. The linear magnetostrictions λ_a and λ_c accompanying a metamagnetic transition are also of opposite signs leading to a small volume magnetostriction. However, they have opposite polarities with respect to the corresponding direction of thermal expansions. In fact, the magnetic contributions to thermal expansion of an antiferromagnet below T_N are suppressed by the opposite polarity corresponding to magnetostrictions caused by the metamagnetic transition.

UAu_2Si_2 belongs to the family of UT_2Si_2 compounds which adopt the tetragonal $ThCr_2Si_2$ structure (UIr_2Si_2 and UPt_2Si_2 crystallize in the $CaBe_2Ge_2$ structure [15]). These compounds exhibit a spectrum of physical properties ranging from Pauli paramagnets (UFe_2Si_2 [16], URe_2Si_2, and UOs_2Si_2 [17]) to magnetically ordered systems which are mostly complex and either AFM (UCr_2Si_2 [18], UCo_2Si_2 [19], UNi_2Si_2 [20], URh_2Si_2 [21], UPd_2Si_2 [21,22], UIr_2Si_2 [17,23], and UPt_2Si_2 [17]), or FM (UMn_2Si_2 [16]). UCu_2Si_2 [19,24–26] exhibits a FM ground state with an additional AFM phase at higher temperatures. An exceptional case among them is the well-known URu_2Si_2 [4] exhibiting the HO transition. The magnetism of UAu_2Si_2 was for many years left unclear mainly due to metallurgical difficulties [15].

Quite recently we have successfully prepared a UAu_2Si_2 single crystal and commenced systematic investigations of its intrinsic properties. The results obtained by measurements of magnetization, specific heat, and electrical resistivity [27] followed by neutron diffraction [28] and ^{29}Si-NMR [29] experiments corroborate the conclusion about the ground state of UAu_2Si_2 as an uncompensated antiferromagnet, contrary to previous reports on polycrystals [17,30–33]. UAu_2Si_2 undergoes a FM-like transition at 50 K (referred to as T_2) followed by another magnetic phase transition (T_m) around 20 K. All our previous measurements show a large magnetocrystalline anisotropy with the direction of magnetic moments along the c axis. The propagation vector is $(2/3, 0, 0)$ and the magnetic structure can be described as a stacking sequence $(+ + -)$ of the FM ac plane sheets along the a axis [28]. Specific-heat measurements point to an enhanced value of the Sommerfeld coefficient $\gamma \sim 180\,\mathrm{mJ\,K^{-2}\,mol^{-1}}$. We investigated the UAu_2Si_2 single crystal by use of thermal-expansion, magnetostriction and magnetization measurements up to high magnetic fields and under hydrostatic pressure. The results of the present paper, are complementary to our previous neutron-diffraction work, confirming the uncompenasted antiferromagnetic (UAFM) ground state of the compound [28], and bring evidence for the intrinsic nature of the FM component below ~50 K previously reported as parasitic in our first single-crystal study [27]. Magnetization measurements in pulsed high magnetic fields helped us to complete the phase diagram of UAu_2Si_2 and revealed signs for the presence of a tricritical point (TCP).

II. EXPERIMENTAL DETAILS

The UAu_2Si_2 single crystal used in this study was prepared using the floating-zone method in an optical furnace (Crystal Systems Co.) in a similar way as in our previous work [27]. Nevertheless, to obtain higher quality and larger single crystals, we have optimized the entire growth process. The initial polycrystalline rod with diameter of 6 mm and length of ~100 mm was prepared from the starting elements of U (initially 99.9% and consequently purified by the Solid State Electrotransport Method under ultrahigh vacuum [34]), Au (99.99%), and Si (99.999%). The rod was subsequently annealed at 1000 °C for three days, cut in two parts, and placed in the optical furnace, where the shorter bottom part served as a polycrystalline seed and the main larger rod hung from the top as feed material for the growth. The chamber of the

optical furnace was evacuated to $\sim 10^{-6}$ mbar and the growth itself was done under protective Ar atmosphere with a flow of $1.5\,l\,\mathrm{min}^{-1}$ in an overpressure of ~0.2 MPa. The power of the lamps in the furnace was adjusted to keep the temperature of the hot zone slightly above the melting point. Both the seed and feed rod were slowly pulled through the hot zone with a speed of $1\,\mathrm{mm\,h}^{-1}$ and without rotation. The quality of the grown single crystal was checked by the x-ray Laue method and energy-dispersive x-ray analysis.

Length changes were measured using a miniature capacitance dilatometer [35] mounted in PPMS 9 T and PPMS 14 T (Quantum Design Co.) between 2 and 100 K in magnetic fields up to 14 T. Magnetization measurements in static fields were done using the vibrating sample magnetometer option implemented in the PPMS 14 T. Specific-heat measurements up to 9 T were performed using the relaxation technique by PPMS 9 T (Quantum Design Co.).

The magnetization in pulsed magnetic fields up to ~58 T was measured at the Dresden High Magnetic Field Laboratory using a coaxial pick-up coil system. The high-field magnetometer is described in Ref. [36]. Absolute values of the magnetization were calibrated using static-field measurements.

The magnetization measurements under hydrostatic pressure were performed in a MPMS SQUID (Quantum Design Co.) magnetometer using a CuBe pressure cell [37] with a liquid pressure medium and a piece of lead as manometer. The heat capacity of the UAu_2Si_2 sample under high pressures was measured by means of steady-state calorimetry [38]. A double-layered CuBe/NiCrAl piston-cylinder pressure cell was used to generate pressures up to ~3 GPa, with a Daphne 7373 pressure medium and a manganin manometer. A micro strain-gauge was used for periodic heating of the sample and an Au/AuFe thermocouple was used to measure its temperature oscillations. The amplitude of oscillations is inversely proportional to the sample heat capacity. Technical details of the method [38,39] and actual experimental setup used in our experiments [40] are beyond the scope of this paper and can be found elsewhere.

III. RESULTS

A. Thermal-expansion measurements

The a- and c-axis linear thermal expansions together with the volume expansion calculated according to Eq. (1) are plotted in Fig. 1. The individual data are vertically shifted to set them equal to 0 at $T_m = 20.5$ K. Below this magnetic phase transition, we observe a significant change in the temperature dependence of the thermal expansion in line with our previous reports [27,28].

There obviously is a large anisotropy of the thermal expansion over the entire temperature range. The linear thermal expansion along the a axis shows a continuous decrease from 100 K down to the ordering temperature $T_m = 20.5$ K, where it bends down rapidly, pointing at a large contraction of the unit cell along the a axis (-1.5×10^{-4} between T_m and 2 K). On the other hand, the thermal expansion along the c axis shows a broad minimum around 75 K followed by an increase at lower temperatures. The ordering temperature appears as an inflection point and the c-axis expansion below 20.5 K is

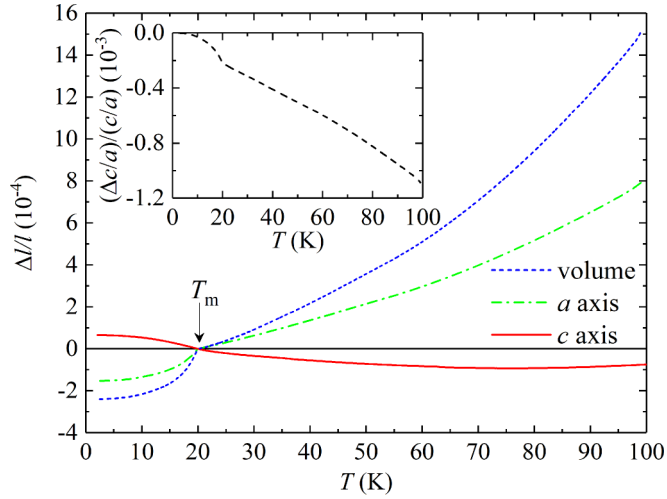

FIG. 1. Linear thermal expansion for the a and c axis and volume change measured without applied external magnetic field. The inset shows c/a as a function of temperature. The curve is normalized to be equal to 0 at 2 K.

6.6×10^{-5}. The volume thermal expansion is calculated using Eq. (1). The obtained relative volume change shows a large reduction below T_m(-2.3×10^{-4} between T_m and 2 K) as shown in Fig. 1. The continuous character of the linear thermal expansion at T_m points to a second-order transition.

The linear thermal-expansion coefficients α_i are defined as temperature derivatives of the linear thermal expansion $(\Delta l/l)_i$, i.e., $\alpha_i = \mathrm{d}(\Delta l/l)_i/\mathrm{d}T$. The calculated linear thermal-expansion coefficients are plotted in Fig. 2 together with the volume thermal-expansion coefficient defined as $\alpha_v = 2\alpha_a + \alpha_c$. It is also useful to determine the temperature dependence of the c/a ratio. We, therefore, define the following temperature coefficient: $\alpha_{c/a} = \alpha_c - \alpha_a$. Both quantities are plotted in Fig. 2.

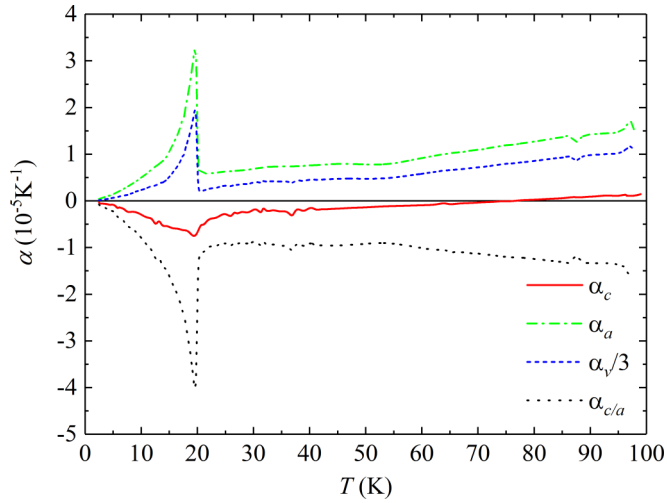

FIG. 2. Linear thermal-expansion coefficients for the a and c axis together with $\alpha_{c/a}$. Note that the volume dependence is plotted as $\alpha_v/3$.

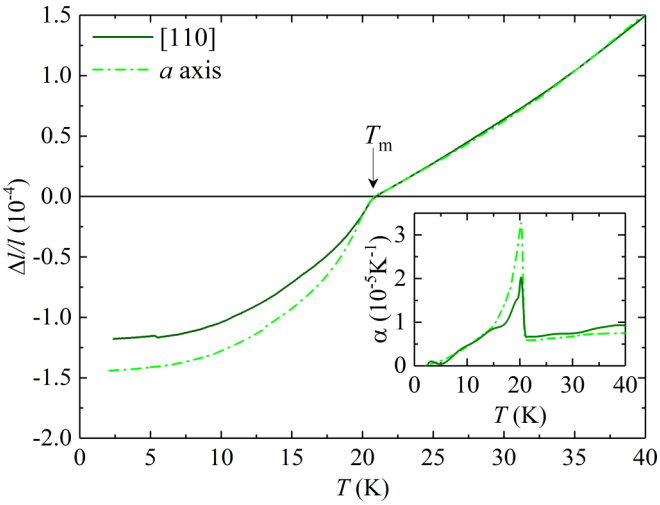

FIG. 3. Linear thermal expansion in the tetragonal plane measured along the a axis and along the [110] direction. The inset shows the corresponding thermal-expansion coefficient for both directions.

The linear thermal-expansion coefficient for the c axis becomes negative below 75 K where the minimum of its relative length change occurs. There are sharp peaks at T_m for all measured curves and a small change of the slope above 50 K visible in α_a that is projected in the remaining computed quantities. Integration of the $\alpha_{c/a}$ coefficient along the whole temperature range results in the relative temperature dependence of the c/a ratio, see inset in Fig. 1.

The temperature dependence of this ratio is monotonous and decreasing nearly linear above T_m. The slope increases below T_m, emphasizing again the prominent contraction of the a axis.

As will be discussed below, ultrapure samples of the isostructural compound URu_2Si_2 studied by synchrotron x-ray diffraction show a small orthorhombic distortion when entering the HO state [41]. The size of the distortion and/or sample quality are possible reasons why it was not observed by thermal-expansion measurements [8,42].

To test the presence of a lattice distortion in UAu_2Si_2, we measured the thermal expansion also along the a axis and [110][1] direction. The corresponding thermal expansions and the linear thermal-expansion coefficients are plotted in Fig. 3.

If the fourfold rotational symmetry of the tetragonal structure of UAu_2Si_2 in the UAFM phase can be broken similar to the case of isostructural URu_2Si_2, the crystal structure itself is expected to have an orthorhombic distortion, lowering the space symmetry. For the $I4/mmm$ space group, two subgroups $Fmmm$ and $Immm$ may have such orthorhombic distortions, but the ab plane primitive vector direction is rotated by 45° (Ref. [41]). In fact, this "orthorhombic" distortion is monoclinic within the original tetragonal unit cell, i.e., with opposite changes of the [110] and [−110] axes. This behavior is not seen in a macroscopic sample under ambient condition, owing to the formation of domains. A small uniaxial pressure applied on multiple domains may change the domain structure toward an orthorhombic monodomain state so that the distortion may be indicated also macroscopically as suggested in case of URu_2Si_2 [43]. That is probably why we could observe the distortion in our dilatometer, which exerts a slight uniaxial pressure along the direction of measurement.

[1]We use Miller indices notation for this direction for its self-explanatory meaning while, for simplicity, a and c are used for the [100] and [001] directions, respectively, throughout the whole paper.

TABLE I. The jumps of the thermal-expansion coefficients $\Delta\alpha_i$ at T_m and the corresponding hydrostatic-pressure and uniaxial-pressure derivatives of T_m predicted using the Ehrenfest relation.

	$\Delta\alpha_i\,(\mathrm{K}^{-1})$	$\frac{dT_m}{dp}\,(\mathrm{K\,GPa}^{-1})$
a	$2.69(8) \times 10^{-5}$	2.7(1)
c	$-4.4(1) \times 10^{-6}$	−0.44(1)
Volume	$4.9(1) \times 10^{-5}$	4.9(1)

The thermodynamic relation for second-order phase transitions known as Ehrenfest relation allows us to estimate the pressure dependence of the ordering temperature based on the jumps in the specific heat ΔC and the thermal-expansion coefficient $\Delta\alpha$ at T_m. It is defined as

$$\frac{dT_m}{dp} = \frac{\Delta\alpha V_m}{\Delta C/T}, \tag{2}$$

and it can serve as an estimation for the hydrostatic-pressure dependence using the volume thermal-expansion coefficient α_v, or for the uniaxial pressure dependences when the linear thermal-expansion coefficients α_a or α_c are used. The jumps of the thermal-expansion coefficients at T_m and the corresponding hydrostatic-pressure and uniaxial-pressure derivatives of T_m predicted using Eq. (2) are shown in Table I.

B. Specific-heat, magnetization, and magnetostriction measurements

First we measured temperature dependences of the specific heat in various magnetic fields applied along the c axis. In Fig. 4, we can indeed see that T_m increases with magnetic field up to ∼4 T, reaching the maximum value between 4 and 5 T and then decreases with further increasing the field.

The magnetization was measured at various temperatures from 2 to 50 K as function of magnetic field up to 14 T applied along the c axis. This was followed by high-field measurements in pulsed magnetic fields up to ∼58 T. The results are shown in Fig. 5. The magnetization data up to 13 K show a low-field inflection point in the hysteretic part of the curve labeled as $\mu_0 H_1$. Another steplike feature is present at higher field and is labeled as $\mu_0 H_2$. Unlike the low-field transition, the $\mu_0 H_2$ anomaly can be traced to temperatures above T_m and is clearly distinguishable even at 40 K. We have discussed this behavior in Ref. [27], especially in the parts connected with Figs. 11, 18–20, therein. Two components apparently coexist at temperatures below T_m: (a) a very weak FM one which emerges around 50 K with cooling; its coercive field $\mu_0 H_2$ increases with decreasing temperature and exceeds 4 T at 2 K, and (b) an uncompensated AFM one (UAFM) with a considerably larger spontaneous magnetization but a much smaller coercive field $\mu_0 H_1$. The magnetization isotherms in the vicinity of T_m show another field-induced steplike

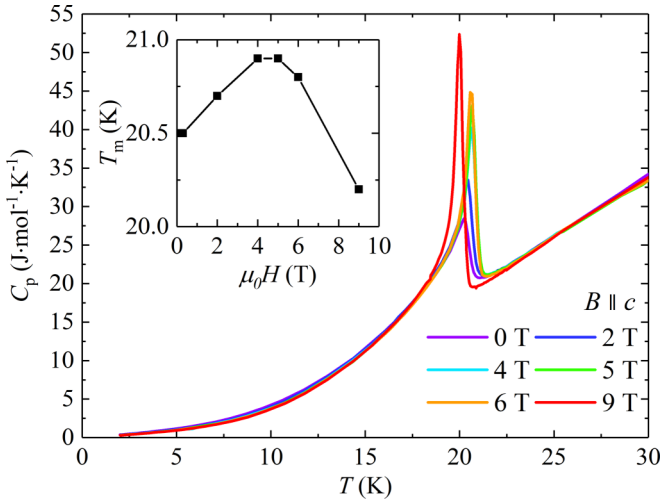

FIG. 4. Temperature dependence of the specific heat of UAu_2Si_2 in magnetic fields applied along the c axis. Inset: Magnetic-field dependence of T_m.

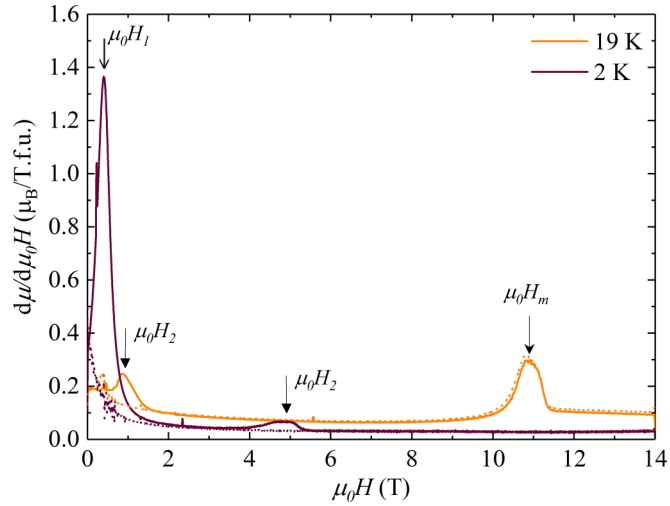

FIG. 6. Field derivatives of the magnetization data at 2 and 19 K depicting the determination of $\mu_0 H_1$, $\mu_0 H_2$, and $\mu_0 H_m$. The solid lines correspond to field-up and dotted lines to field-down sweeps.

transition at higher fields. Similar transitions were observed in our previous work on a different single crystal [27]. There, the anomalies labeled as $\mu_0 H_m$ were, however, much less pronounced, probably due to lower crystal quality. The values of the characteristic fields at different temperatures have been determined using plots of $\mathrm{d}\mu/\mathrm{d}\mu_0 H$ vs. $\mu_0 H$ shown in Fig. 6 for results at 2 and 19 K.

Further magnetization measurements in pulsed fields were performed to track the metamagnetic transition $\mu_0 H_m$. The measured magnetization was scaled using the static-field data obtained at 2 K and a small linear background was subtracted to give the correct absolute values. Results of the high-field measurement are plotted in Fig. 7. A clear metamagnetic transition at $\mu_0 H_m$ is visible on all measured isotherms up to 20.1 K. The metamagnetic transition is most probably of

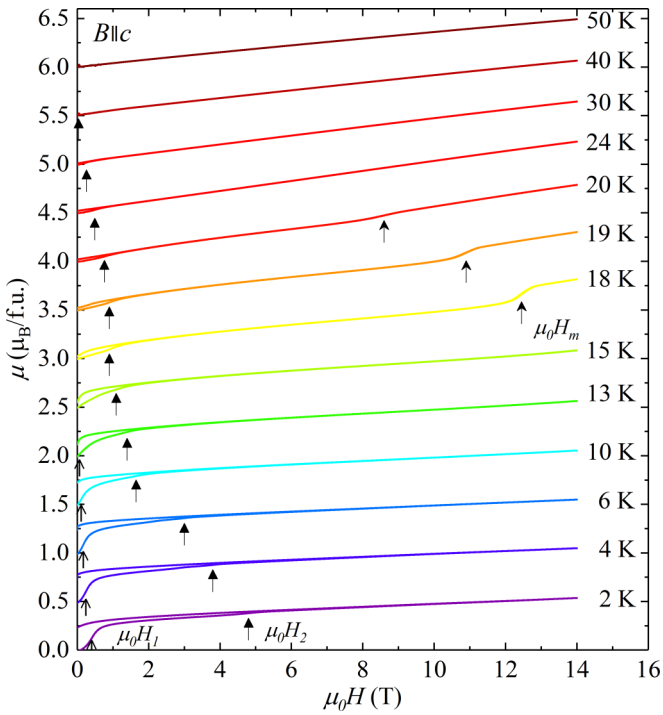

FIG. 5. Magnetization curves measured with the field applied along the c axis up to 14 T. The curves are consecutively shifted by 0.5 μ_B/f.u. along the magnetization axis. The three types of arrows mark $\mu_0 H_1$, $\mu_0 H_2$, and $\mu_0 H_m$, respectively.

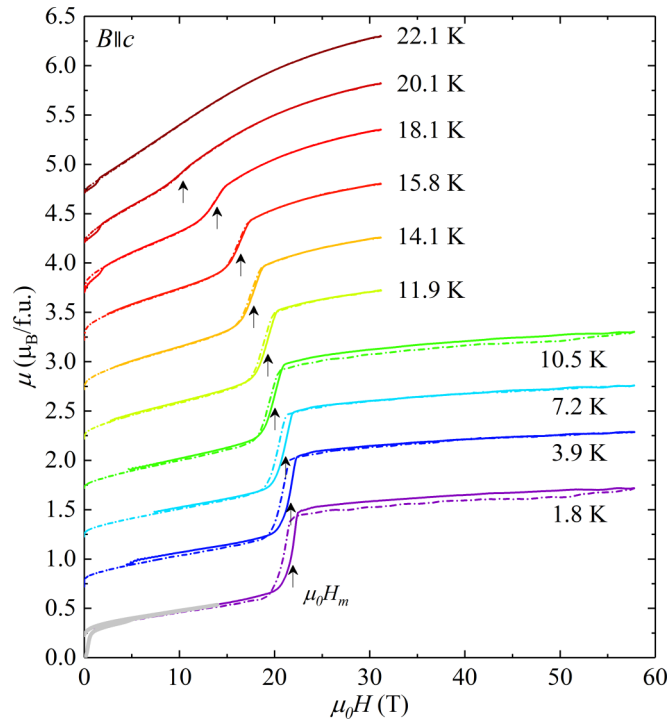

FIG. 7. Magnetization measured in pulsed fields applied along the c axis up to $\approx$ 58 T. The curves are consecutively vertically shifted by 0.5 μ_B/f.u.. The solid lines correspond to field-up and dash-dotted lines to field-down sweeps. The arrows mark the $\mu_0 H_m$ transitions. The gray curve overlapping data at 1.8 K are the static-field data at 2 K up to 14 T shown in Fig. 5.

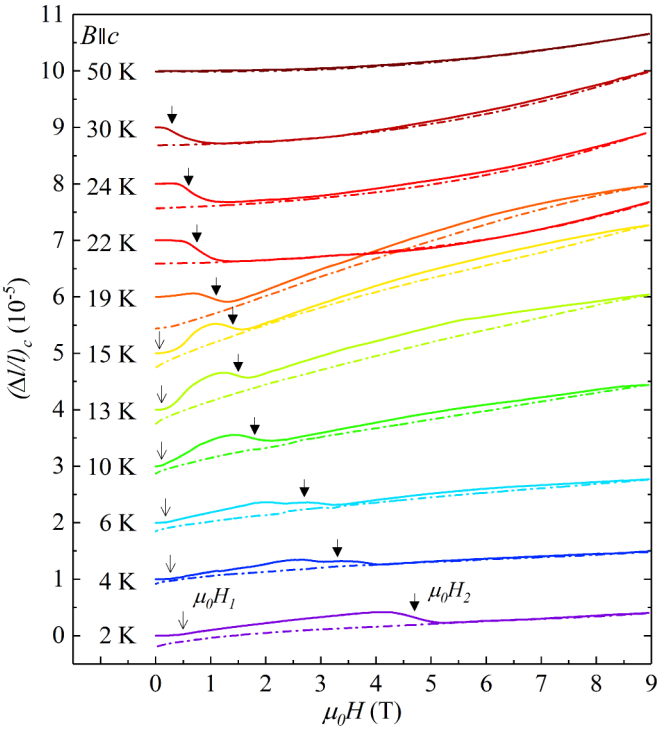

FIG. 8. Longitudinal magnetostriction measured along the c axis. The solid lines correspond to field-up sweeps and dash-dotted lines to field-down sweeps. The curves are vertically shifted for better clarity.

spin-flip type [44], as one would expect for a system with large magnetocrystalline anisotropy. The low-temperature curves also show significant hystereses ($\Delta\mu_0 H_m$) between the up and down sweeps. The hysteresis narrows with increasing temperature and disappears around 16 K when $\mu_0 H_m \sim 16$ T. The temperature dependence of $\Delta\mu_0 H_m$ is shown in Fig. 12.

The longitudinal magnetostriction was measured at various temperatures with magnetic fields up to 9 T applied along the tetragonal c axis, see Fig. 8.

Figure 9 shows how the coercive fields $\mu_0 H_1$ and $\mu_0 H_2$ were determined from the magnetostriction data.

There is a significant change of the shape of the magnetostriction curves when UAu_2Si_2 crosses $T_m = 20.5$ K, going from a concave to a convex curvature. We have consequently conducted further measurements of the longitudinal magnetostriction along the c axis up to 14 T at selected temperatures close to T_m. These isotherms show the high-field anomaly as a pronounced sharp drop at $\mu_0 H_m$ (see Fig. 10), as determined from the magnetization measurements.

We have also measured the temperature dependence of the magnetization in various fields up to 14 T applied along the c axis. These data agree with our previous results obtained on a different single crystal [27]. We can clearly see the anomaly labeled as T_m, determined from the upturn of the magnetization for curves below 5 T and from the peak at higher fields. There is also another transition marked as T_2 that can be distinguished only in the low-field data at 0.1 T (see Fig. 11).

The whole set of anomalies observed in the magnetization, magnetostriction, and thermal-expansion measurements

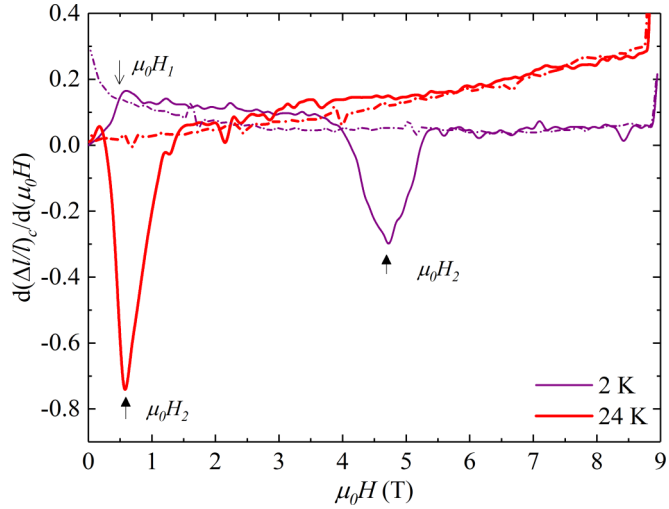

FIG. 9. Field derivatives of the magnetostriction data at 2 and 24 K showing the determination of $\mu_0 H_1$ and $\mu_0 H_2$. The solid lines correspond to field-up and dash-dotted lines to field-down sweeps.

allows us to construct the magnetic phase diagram as plotted in Fig. 12 together with the temperature dependence of the hystereses at $\mu_0 H_1$, $\mu_0 H_2$, and $\mu_0 H_m$.

C. Hydrostatic pressure study

As our calculations using the Ehrenfest relation predict a rather dramatic positive effect of hydrostatic pressure on the ordering temperature ($\approx 4.9(1)$ K GPa^{-1}), we wanted to verify this hypothesis. For that purpose, we measured the magnetization in a field of 0.1 T applied along the c axis under hydrostatic pressures up to ~1 GPa (see Fig. 13). The measured data were corrected for the diamagnetic contribution of the pressure cell. The shape of the ambient-pressure curve differs from those obtained under pressure. This can be an effect of a slightly different orientation of the sample in the pressure cell. Contrary to our prediction, we observe

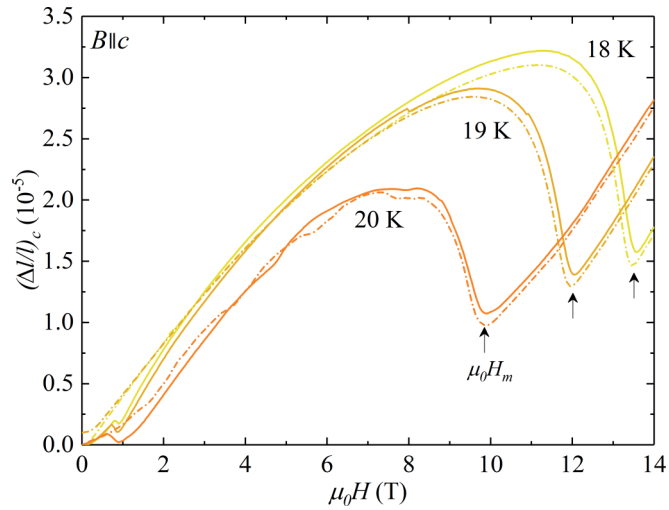

FIG. 10. Longitudinal magnetostriction measured with fields up to the 14 T applied along the c axis.

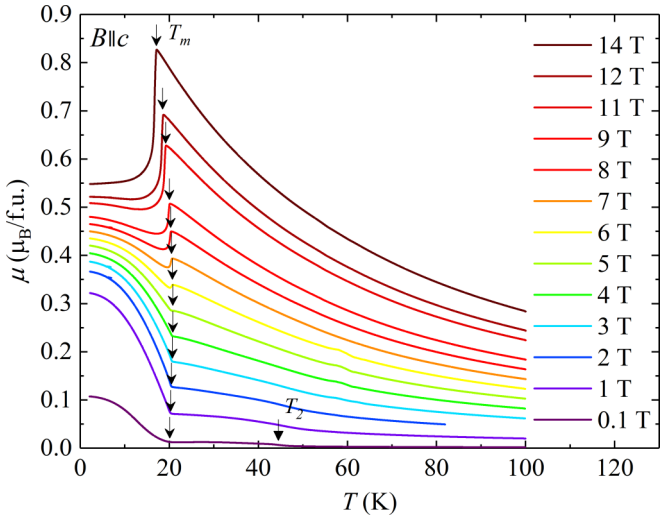

FIG. 11. Temperature dependence of the magnetization along the c axis. The arrows mark the T_m and T_2 transitions.

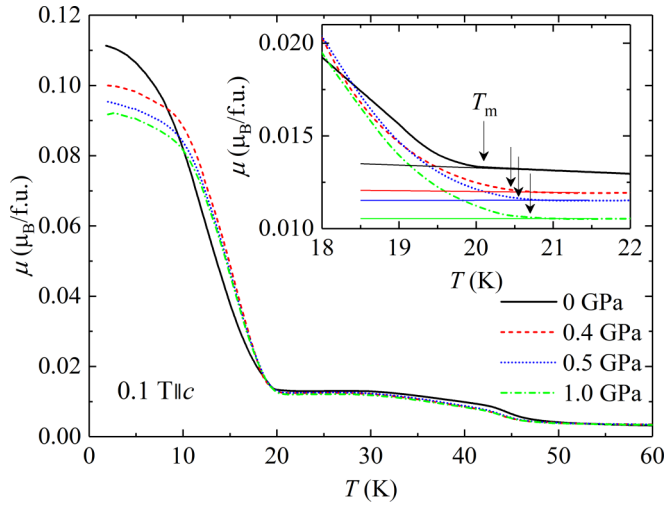

FIG. 13. Magnetization in a magnetic field of 0.1 T applied along the c axis under various hydrostatic pressures up to 1.0 GPa. The inset shows the region near T_m marked by the arrows. The curves in the inset are vertically shifted for clarity.

only a small shift of the transition temperature T_m with applied pressure (see inset of Fig. 13). The transition temperature T_m again is defined by the upturn of the magnetization curve. The resulting small ratio of the pressure change of the ordering temperature is $dT_m/dp \approx 0.6(1)\,\mathrm{K\,GPa^{-1}}$. A larger effect is visible in the reduction of the spontaneous magnetic moment μ_{spont} with the slope $d\mu_{spont}/dp \approx -0.019(6)\,\mu_B/(\mathrm{f.u.\,GPa})$.

The temperature dependence of the specific heat measured under hydrostatic pressure up to 2.79 GPa confirmed that T_m slightly increases with applying pressure of 1 GPa and then decreases at gradually increasing rate with higher pressure (see Fig. 14). The total change of T_m between ambient pressure and 2.79 GPa amounts only -0.4 K, i.e., $\sim -2\%$. In any case the results of our measurements of the pressure influence on T_m strongly contradict the predictions from the Ehrenfest relation. This contradiction obviously requires further studies. At this stage, we can only speculate that the reason can be in a complex hierarchy of exchange interactions.

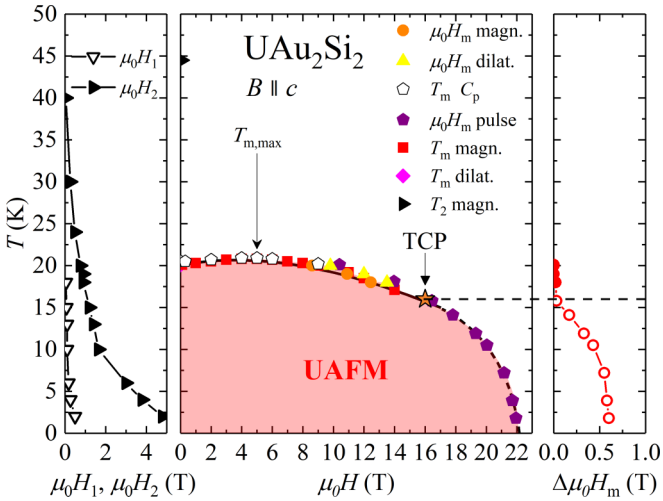

FIG. 12. Middle panel: Magnetic phase diagram of UAu_2Si_2 constructed using the results of the specific-heat—C_p, magnetization, and dilatometric (thermal expansion, magnetostriction) measurements. The star marks the tricritical point—TCP. Left panel: Temperature dependences of μ_0H_1 and μ_0H_2. Right panel: Temperature dependence of the hysteresis of the metamagnetic transition μ_0H_m resulting from the pulsed-field measurements—open symbols and from the static-field measurements—full symbols.

IV. DISCUSSION

Our thermal-expansion measurements on a UAu_2Si_2 single crystal revealed a large anisotropy which is mainly due to magnetic contributions. The ordered state below T_m is connected with a dramatic lattice contraction in the basal plane (a axis). This together with the relatively small expansion of the c axis leads to the ground-state volume collapse (Fig. 1). This behavior strongly resembles the case of the isostructural

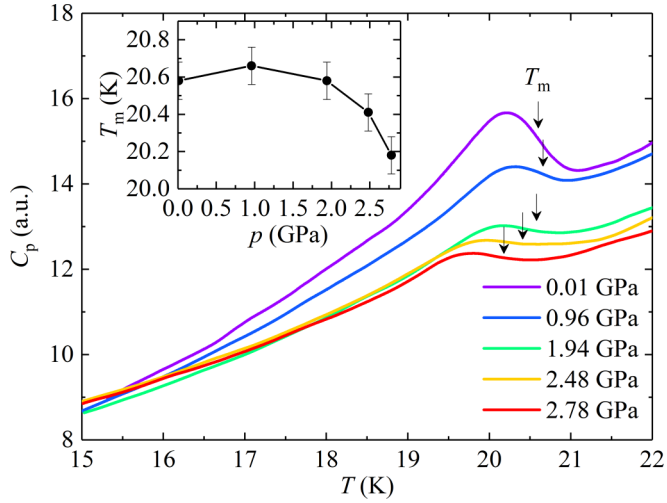

FIG. 14. Temperature dependence of the specific heat of UAu_2Si_2 under hydrostatic pressure. Inset: Pressure dependence of T_m.

heavy-fermion compound URu_2Si_2 entering the HO state at 17.5 K [8]. The linear thermal-expansion coefficient for the a axis consequently exhibits a sharp positive anomaly at the ordering temperature whereas the c-axis anomaly is negative and less pronounced (Fig. 2). The volume thermal-expansion coefficient of URu_2Si_2 also exhibits a sharp and positive peak at 17.5 K that can be translated to a volume decrease in the ground state. A very similar behavior for both compounds can be found in the temperature dependence of the c/a ratio. Both materials show an upturn below the ordering temperature, accenting the contraction in the basal plane, and nearly linear temperature dependence at higher temperatures up to 40 K. Nevertheless, the c/a ratio of URu_2Si_2 has a pronounced minimum around 60 K, that is not visible for UAu_2Si_2, which shows a linear temperature dependence up to 100 K. Even though the overall character of the thermal expansion of URu_2Si_2 and UAu_2Si_2 is qualitatively similar, it does differ quantitatively. The step in the volume thermal-expansion coefficient $\alpha_v^* = (\alpha_a + \alpha_b + \alpha_c)/3$ is $\sim 2.5 \times 10^{-6}\,K^{-1}$ for URu_2Si_2 [8] and almost an order of magnitude larger ($\sim 1.6 \times 10^{-5}\,K^{-1}$) for UAu_2Si_2. It is believed, that anomalies in the thermal-expansion coefficient of the order of 10^{-4}, 10^{-5} can be connected with a structural transition [8], as in the case of UPd_3 [45]. In that sense, URu_2Si_2 does not evidence a structural change in the HO state. Nevertheless, there is a list of studies which suggests the breaking of the fourfold rotational symmetry of the tetragonal c axis [46–51], whereas high-resolution x-ray backscattering [52] and thermal-expansion data [8,42] do not confirm this. However, lattice-symmetry breaking from the fourfold tetragonal to twofold orthorhombic structure was unambiguously observed by high-resolution synchrotron x-ray diffraction measurements in zero field [41]. The fact that this distortion is observed only in ultrapure samples may explain the long list of more or less unsuccessful attempts to observe this.

As the thermal-expansion coefficients of UAu_2Si_2 are even one order of magnitude larger (i.e., $\sim 10^{-5}$), the possibility of some kind of lattice distortion should be seriously considered. Our thermal-expansion measurements show an anisotropic expansion in the basal plane breaking the fourfold symmetry along the c axis. The body-centered room-temperature tetragonal structure of UAu_2Si_2 belongs to the $I4/mmm$ space group. It has 15 maximal nonisomorphic subgroups and only two of them have no fourfold symmetry along the c axis. These are the orthorhombic $Fmmm$ and $Immm$ space groups. The same space groups were also considered in the synchrotron x-ray diffraction study of URu_2Si_2 [41]. The $Fmmm$ space group was found to describe the system in the HO state.

The measurement of thermal expansion, as a macroscopic quantity, is not sufficient to properly describe the space group of the distorted structure, even though it is more sensitive to detect distortions than diffraction studies. In that sense, high-resolution x-ray diffraction experiments are needed to resolve the structure of UAu_2Si_2 in the ordered state. Our results from an ultrasonic study show a Curie-type softening in the transverse $(C_{11} - C_{12})/2$ mode toward T_m, that could also point to orthorhombic distortion at T_m [53]. In analogy with URu_2Si_2, where also a softening of the same mode was observed suggesting that the $\Gamma_{3g}(B_{1g})$-type lattice instability is innate in these systems [42,54].

The large ground-state volume collapse of UAu_2Si_2 indicates an initial positive pressure dependence of the ordering temperature of $dT_m/dp \approx 4.9(1)\,K\,GPa^{-1}$, according to the Ehrenfest relation. Uniaxial pressure applied along the a axis should have a positive effect as well ($\approx 2.7(1)\,K\,GPa^{-1}$). On the other hand, uniaxial pressure along the tetragonal c axis should lower T_m at a rate of $\approx -0.44(1)\,K\,GPa^{-1}$. These findings qualitatively agree with the experimentally confirmed behavior of URu_2Si_2 where the predicted pressure dependences are approximately eight times smaller. Ehrenfest-relation estimates give a pressure dependence of the HO transition of $1.4\,K\,GPa^{-1}$ (Ref. [8]) and high-pressure resistivity measurements show an experimental initial slope of $1.01\,K\,GPa^{-1}$ (Ref. [55]). The estimated pressure changes of the ordering temperature of the HO of URu_2Si_2 and the UAFM state of UAu_2Si_2 are largely different. A similar dramatic change of the dT/dp values was observed for the $U(Ru, Fe)_2Si_2$ system, where doping of Fe leads to a change of the HO to "large-moment antiferromagnetism" [11]. However, our measurement of the magnetization under hydrostatic pressure up to 1.0 GPa shows only a weak pressure dependence of T_m (Fig. 13). The estimated slope is $dT_m/dp \approx 0.6(1)\,K\,GPa^{-1}$. We also observed the lowering of the spontaneous magnetization with increasing pressure $d\mu_{spont}/dp \approx -0.019(6)\,\mu_B/(f.u.\,GPa)$. The specific-heat measurement under hydrostatic pressure up to 2.79 GPa revealed a small initial increase of T_m up to 1 GPa followed by a suppression for higher pressure. The observed inconsistency with the expected trend from the Ehrenfest relation is rather unexpected. It may be caused by a structural distortion that takes place at T_m. In that case, Eq. (1) is not valid and the real volume change can be different, i.e., possibly smaller. Another question is the applicability of the Ehrenfest relation itself. Although it is widely and successfully used to characterize the pressure dependence (both positive and negative) of AFM [56,57] and FM [56,58,59] second-order phase transitions, it may strictly be applied only for the superconducting transitions [60]. And even for some superconductors, the predicted pressure dependence determined by use of the Ehrenfest relation differs from the experimental findings, such as in the case of $PuCoGa_5$ [61] by an order of magnitude or even by sign in the layered iron-based superconductors of the $Ba(Fe_{1-x}Co_x)_2As_2$ series [62]. Both of these systems exhibit very anisotropic thermal-expansion coefficients, similar as for UAu_2Si_2.

The magnetization isotherms (Figs. 5 and 7) clearly and reproducibly show anomalies at $\mu_0 H_1$, $\mu_0 H_2$, and $\mu_0 H_m$ in line with our previous study on a different single crystal. However, we now find a much sharper character of the steplike transition at $\mu_0 H_m$. We suggest that the deviation from the linear dependence of the magnetization that was marked as $\mu_0 H_m$ in our previous work [27], is a low-field sign of the steplike transition which takes place at higher fields. We have previously not observed this transition, possibly due to a lower crystal quality or slightly improper orientation of the c axis with respect to the applied field.

Our magnetostriction measurements (Figs. 8 and 10) with field applied along the c axis reproduce the anomalies observed in the magnetization data. The transition at T_2 is reflected in the thermal-expansion data only by a small slope change in α_a, α_v, and $\alpha_{c/a}$ around 50 K (Fig. 2). The size

of the relative length change of the c axis at the $\mu_0 H_2$ anomaly is of the order of 10^{-6}. This provides evidence of its bulk character, which can be traced up to ∼40 K as in the magnetization data. A larger relative length contraction ($\sim 10^{-5}$) takes place at $\mu_0 H_m$. It resembles the c-axis contraction at the field-induced phase transition of URu_2Si_2 [63].

Our high-field magnetization measurements show that the temperature dependence of the hysteresis of the $\mu_0 H_m$ transition vanishes around 16 K (and 16 T) where the transition changes its character from steplike to continuous. This is attributed to the change of the order of the phase transition from first order (in higher fields) to second order (in lower fields). Such a point is usually referred to as a TCP [44]. We marked this point by a star in the phase diagram in Fig. 12. Similar TCPs have recently been reported in the uranium-based antiferromagnets USb_2 [64] and UN [65]. The critical field, where the transition temperature T_m is suppressed to 0 K in UAu_2Si_2 is extrapolated to be about 22 T.

V. CONCLUSIONS

Our thermal-expansion, specific-heat, magnetostriction, and magnetization study allowed us to complete a comprehensive magnetic phase diagram for UAu_2Si_2.

The magnetostriction curves measured at higher temperatures confirm bulk character of the 50 K weak FM phase. The large volume contraction in the UAFM ordered state suggests a large positive pressure dependence of T_m. The linear thermal-expansion data point on the opposite effect for uniaxial pressure applied along the tetragonal c axis and within the basal plane. Magnetization measurements in a hydrostatic pressure cell, however, revealed a negligible hydrostatic pressure effect on T_m, namely $dT_m/dp \approx 0.6(1)\,\mathrm{K\,GPa^{-1}}$ in pressures up to 1.0 GPa. A small initial increase of T_m under hydrostatic pressure up to 1 GPa was observed in the specific-heat data, while a continuous decrease is found for higher pressures up to 2.79 GPa. These values are much smaller than the prediction from the Ehrenfest relations ($dT_m/dp \approx 4.9(1)\,\mathrm{K\,GPa^{-1}}$). Further complex studies involving hydrostatic and uniaxial pressure would be desired to shed more light on the nature of this controversy.

As the order of all the relative length changes is $\sim 10^{-5}$, we can expect some structural changes or distortions of the UAu_2Si_2 unit cell in the ground state. Our comparative dilatometry measurements of the linear thermal expansion along the a axis and along the [110] direction clearly show the fourfold symmetry breaking in the basal plane. This may also affect the real low-pressure dependence of the ordering temperature. High-resolution diffraction measurements are needed to find the ground-state space group. Possible candidates are the orthorhombic nonisomorphic subgroups $Fmmm$ and $Immm$, where the first one was found to describe the structure of the high-quality samples of URu_2Si_2 in the HO state. Our high-field magnetization measurements revealed a critical field of ≈ 22 T where the ordering temperature T_m is suppressed to 0 K. The hysteresis of this transition emerges at a TCP given by $T_m \approx 16$ K and $\mu_0 H_m \approx 16$ T as a sign of the change of the transition from second to first order.

ACKNOWLEDGMENTS

The present research was supported by JSPS KAKENHI Grants No. JP17K05525, No. JP15KK0146, No. JP15K05882, No. JP15K21732, and the Strategic Young Researcher Overseas Visits Program for Accelerating Brain Circulation from JSPS. Single crystal growth and the majority of experiments were performed in the Materials Growth and Measurement Laboratory MGML (see http://mgml.eu). We acknowledge the support of HLD at HZDR, a member of the European Magnetic Field Laboratory (EMFL), where the magnetization measurements in high-pulsed fields have been done. We would like to thank Sergei Zherlitsyn for his help during the high-field magnetization measurement.

[1] D. D. Koelling, B. D. Dunlap, and G. W. Crabtree, Phys. Rev. B **31**, 4966 (1985).
[2] J. L. Smith and E. A. Kmetko, J. Less-Common Met. **90**, 83 (1983).
[3] O. Eriksson, M. S. S. Brooks, B. Johansson, R. C. Albers, and A. M. Boring, J. Appl. Phys. **69**, 5897 (1991).
[4] T. T. M. Palstra, A. A. Menovsky, J. van den Berg, A. J. Dirkmaat, P. H. Kes, G. J. Nieuwenhuys, and J. A. Mydosh, Phys. Rev. Lett. **55**, 2727 (1985).
[5] M. B. Maple, J. W. Chen, Y. Dalichaouch, T. Kohara, C. Rossel, M. S. Torikachvili, M. W. McElfresh, and J. D. Thompson, Phys. Rev. Lett. **56**, 185 (1986).
[6] W. Schlabitz, J. Baumann, B. Pollit, U. Rauchschwalbe, H. M. Mayer, U. Ahlheim, and C. D. Bredl, Zeitschrift für Physik B Condensed Matter **62**, 171 (1986).
[7] J. A. Mydosh and P. M. Oppeneer, Rev. Mod. Phys. **83**, 1301 (2011).
[8] A. de Visser, F. E. Kayzel, A. A. Menovsky, J. J. M. Franse, J. van den Berg, and G. J. Nieuwenhuys, Phys. Rev. B **34**, 8168 (1986).
[9] A. de Visser, J. J. M. Franse, and J. Flouquet, Physica B **161**, 324 (1990).
[10] G. Motoyama, N. Yokoyama, A. Sumiyama, and Y. Oda, J. Phys. Soc. Jpn. **77**, 123710 (2008).
[11] S. Ran, C. T. Wolowiec, I. Jeon, N. Pouse, N. Kanchanavatee, B. D. White, K. Huang, D. Martien, T. DaPron, D. Snow, M. Williamsen, S. Spagna, P. S. Riseborough, and M. B. Maple, Proc. Natl. Acad. Sci. **113**, 13348 (2016).
[12] A. V. Andreev, Y. Skourski, D. I. Gorbunov, and K. Prokeš, Physica B **536**, 567 (2017).
[13] A. V. Andreev, S. Yasin, Y. Skourski, A. A. Zvyagin, S. Zherlitsyn, and J. Wosnitza, Phys. Rev. B **87**, 214409 (2013).
[14] F. Honda, G. Oomi, A. V. Andreev, V. Sechovský, and A. A. Menovsky, Physica B **259–261**, 256 (1999).
[15] V. Sechovsky and L. Havela, Magnetism of ternary intermetallic compounds of uranium, in *Handbook of Magnetic Materials* (Elsevier, Amsterdam, 1998), Vol. 11, Chap. 1, pp. 1289.
[16] A. Szytuka, S. Siek, J. Leciejewicz, A. Zygmunt, and Z. Ban, J. Phys. Chem. Solids **49**, 1113 (1988).
[17] T. T. M. Palstra, A. A. Menovsky, G. J. Nieuwenhuys, and J. A. Mydosh, J. Magn. Magn. Mater. **54–57**, 435 (1986).
[18] T. D. Matsuda, N. Metoki, Y. Haga, S. Ikeda, K. Kaneko, E. Yamamoto, and Y. Onuki, J. Phys.: Condens. Matter **15**, S2023 (2003).

[19] L. Chełmicki, J. Leciejewicz, and A. Zygmunt, J. Phys. Chem. Solids **46**, 529 (1985).

[20] L. Chełmicki, J. Leciejewicz, and A. Zygmunt, Solid State Commun. **48**, 177 (1983).

[21] H. Ptasiewicz-Bak, J. Phys. F: Met. Phys. **11**, 1225 (1981).

[22] T. Honma, H. Amitsuka, S. Yasunami, K. Tenya, T. Sakakibara, H. Mitamura, T. Goto, G. Kido, S. Kawarazaki, Y. Miyako, K. Sugiyama, and M. Date, J. Phys. Soc. Jpn. **67**, 1017 (1998).

[23] A. J. Dirkmaat, T. Endstra, E. A. Knetsch, G. J. Nieuwenhuys, J. A. Mydosh, A. A. Menovsky, F. R. de Boer, and Z. Tarnawski, Phys. Rev. B **41**, 2589 (1990).

[24] T. D. Matsuda, Y. Haga, S. Ikeda, A. Galatanu, E. Yamamoto, H. Shishido, M. Yamada, J.-I. Yamaura, M. Hedo, Y. Uwatoko, T. Matsumoto, T. Tada, S. Noguchi, T. Sugimoto, K. Kuwahara, K. Iwasa, M. Kohgi, R. Settai, and Y. Ōnuki, J. Phys. Soc. Jpn. **74**, 1552 (2005).

[25] F. Honda, N. Metoki, T. D. Matsuda, Y. Haga, and Y. Ōnuki, J. Phys.: Condens. Matter **18**, 479 (2006).

[26] R. Troć, M. Samsel-Czekała, J. Stępień-Damm, and B. Coqblin, Phys. Rev. B **85**, 224434 (2012).

[27] C. Tabata, N. Miura, K. Uhlířová, M. Vališka, H. Saito, H. Hidaka, T. Yanagisawa, V. Sechovský, and H. Amitsuka, Phys. Rev. B **94**, 214414 (2016).

[28] C. Tabata, M. Klicpera, B. Ouladdiaf, H. Saito, M. Vališka, K. Uhlířová, N. Miura, V. Sechovský, and H. Amitsuka, Phys. Rev. B **96**, 214442 (2017).

[29] C. Tabata, Y. Ihara, S. Shimmura, N. Miura, H. Hidaka, T. Yanagisawa, and H. Amitsuka, J. Phys. Soc. Jpn. **87**, 114707 (2018).

[30] L. Rebelsky, M. W. McElfresh, M. S. Torikachvili, B. M. Powell, and M. B. Maple, J. Appl. Phys. **69**, 4810 (1991).

[31] M. S. Torikachvili, R. F. Jardim, C. C. Becerra, C. H. Westphal, A. Paduan-Filho, V. M. Lopez, and L. Rebelsky, J. Magn. Magn. Mater. **104–107**, 69 (1992).

[32] K. J. Lin, J. S. Hwang, C. S. Wur, R. Hsu, and C. Tien, Solid State Commun. **103**, 185 (1997).

[33] M. Saran and S. P. McAlister, J. Magn. Magn. Mater. **75**, 345 (1988).

[34] Y. Haga, T. Honma, E. Yamamoto, H. Ohkuni, Y. Ōnuki, M. Ito, and N. Kimura, Jpn. J. Appl. Phys. **37**, 3604 (1998).

[35] M. Rotter, M. Doerr, M. Zschintzsch, A. Lindbaum, H. Sassik, and G. Behr, J. Magn. Magn. Mater. **310**, 1383 (2007).

[36] Y. Skourski, M. D. Kuz'min, K. P. Skokov, A. V. Andreev, and J. Wosnitza, Phys. Rev. B **83**, 214420 (2011).

[37] J. Kamarád, Z. Machátová, and Z. Arnold, Rev. Sci. Instrum. **75**, 5022 (2004).

[38] P. F. Sullivan and G. Seidel, Phys. Rev. **173**, 679 (1968).

[39] Y. Kraftmakher, *Modulation Calorimetry: Theory and Applications* (Springer, Berlin, 2004).

[40] M. Míšek, Magnetic and transport properties of f-electron compounds under extreme conditions, Ph.D. thesis, Charles University, 2013.

[41] S. Tonegawa, S. Kasahara, T. Fukuda, K. Sugimoto, N. Yasuda, Y. Tsuruhara, D. Watanabe, Y. Mizukami, Y. Haga, T. D. Matsuda, E. Yamamoto, Y. Onuki, H. Ikeda, Y. Matsuda, and T. Shibauchi, Nat. Commun. **5**, 4188 (2014).

[42] K. Kuwahara, H. Amitsuka, T. Sakakibara, O. Suzuki, S. Nakamura, T. Goto, M. Mihalik, A. Menovsky, A. de Visser, and J. M. Franse, J. Phys. Soc. Jpn. **66**, 3251 (1997).

[43] S. Kambe, D. Aoki, B. Salce, F. Bourdarot, D. Braithwaite, J. Flouquet, and J. P. Brison, Phys. Rev. B **87**, 115123 (2013).

[44] E. Stryjewski and N. Giordano, Adv. Phys. **26**, 487 (1977).

[45] H. R. Ott, K. Andres, and P. H. Schmidt, Physica B+C **102**, 148 (1980).

[46] R. Okazaki, T. Shibauchi, H. J. Shi, Y. Haga, T. D. Matsuda, E. Yamamoto, Y. Onuki, H. Ikeda, and Y. Matsuda, Science **331**, 439 (2011).

[47] T. Shibauchi, H. Ikeda, and Y. Matsuda, Philos. Mag. **94**, 3747 (2014).

[48] S. Tonegawa, K. Hashimoto, K. Ikada, Y. H. Lin, H. Shishido, Y. Haga, T. D. Matsuda, E. Yamamoto, Y. Onuki, H. Ikeda, Y. Matsuda, and T. Shibauchi, Phys. Rev. Lett. **109**, 036401 (2012).

[49] S. Tonegawa, K. Hashimoto, K. Ikada, Y. Tsuruhara, Y. H. Lin, H. Shishido, Y. Haga, T. D. Matsuda, E. Yamamoto, Y. Onuki, H. Ikeda, Y. Matsuda, and T. Shibauchi, Phys. Rev. B **88**, 245131 (2013).

[50] S. Kambe, Y. Tokunaga, H. Sakai, T. D. Matsuda, Y. Haga, Z. Fisk, and R. E. Walstedt, Phys. Rev. Lett. **110**, 246406 (2013).

[51] S. C. Riggs, M. C. Shapiro, A. V. Maharaj, S. Raghu, E. D. Bauer, R. E. Baumbach, P. Giraldo-Gallo, M. Wartenbe, and I. R. Fisher, Nat. Commun. **6**, 6425 (2015).

[52] C. Tabata, T. Inami, S. Michimura, M. Yokoyama, H. Hidaka, T. Yanagisawa, and H. Amitsuka, Philos. Mag. **94**, 3691 (2014).

[53] T. Yanagisawa (unpublished).

[54] T. Yanagisawa, S. Mombetsu, H. Hidaka, H. Amitsuka, M. Akatsu, S. Yasin, S. Zherlitsyn, J. Wosnitza, K. Huang, and M. Brian Maple, J. Phys. Soc. Jpn. **82**, 013601 (2012).

[55] E. Hassinger, G. Knebel, K. Izawa, P. Lejay, B. Salce, and J. Flouquet, Phys. Rev. B **77**, 115117 (2008).

[56] J. J. Neumeier, A. L. Cornelius, and K. Andres, Phys. Rev. B **64**, 172406 (2001).

[57] G. M. Schmiedeshoff, S. M. Hollen, S. L. Bud'ko, and P. C. Canfield, AIP Conf. Proc. **850**, 1297 (2006).

[58] A. Gasparini, Y. K. Huang, J. Hartbaum, H. v. Löhneysen, and A. de Visser, Phys. Rev. B **82**, 052502 (2010).

[59] S. Sakarya, N. H. van Dijk, A. de Visser, and E. Brück, Phys. Rev. B **67**, 144407 (2003).

[60] A. Pippard, *Elements of Classical Thermodynamics: For Advanced Students of Physics* (Cambridge University Press, Cambridge, 1964).

[61] R. Eloirdi, C. Giacobbe, P. A. Celdran, N. Magnani, G. H. Lander, J. C. Griveau, E. Colineau, K. Miyake, and R. Caciuffo, Phys. Rev. B **95**, 094517 (2017).

[62] M. S. da Luz, J. J. Neumeier, R. K. Bollinger, A. S. Sefat, M. A. McGuire, R. Jin, B. C. Sales, and D. Mandrus, Phys. Rev. B **79**, 214505 (2009).

[63] V. F. Correa, S. Francoual, M. Jaime, N. Harrison, T. P. Murphy, E. C. Palm, S. W. Tozer, A. H. Lacerda, P. A. Sharma, and J. A. Mydosh, Phys. Rev. Lett. **109**, 246405 (2012).

[64] R. L. Stillwell, I. L. Liu, N. Harrison, M. Jaime, J. R. Jeffries, and N. P. Butch, Phys. Rev. B **95**, 014414 (2017).

[65] K. Shrestha, D. Antonio, M. Jaime, N. Harrison, D. S. Mast, D. Safarik, T. Durakiewicz, J. C. Griveau, and K. Gofryk, Sci. Rep. **7**, 6642 (2017).